LETTER Communicated by Thomas Bartol

Molecular Diffusion Model of Neurotransmitter Homeostasis Around Synapses Supporting Gradients

Ashwin Mohan
amgc5@mizzou.edu
Sandeep Pendyam
sppm7@mizzou.edu
Department of Electrical and Computer Engineering, University of Missouri, Columbia, MO 65211, U.S.A.

Peter W. Kalivas
kalivasp@musc.edu
Department of Neurosciences, Medical University of South Carolina, Charleston, SC 29425, U.S.A.

Satish S. Nair
nairs@missouri.edu
Department of Electrical and Computer Engineering, University of Missouri, Columbia, MO 65211, U.S.A.

Neurotransmitter homeostasis in and around a synapse involves complex random processes such as diffusion, molecular binding, and uptake by glial transporters. A three-dimensional stochastic diffusion model of a synapse was developed to provide molecular-level details of neurotransmitter homeostasis not predicted by alternative models based on continuum approaches. The development was illustrated through an example case cortico-accumbens synapse that successfully integrated neuroadaptations observed after chronic cocaine. By incorporating cystine-glutamate exchanger as a nonsynaptic release site for glutamate, the stochastic model was used to quantify the relative contributions of synaptic and nonsynaptic sources to extracellular concentration and to estimate molecular influx rates into the perisynapse. A perturbation analysis showed that among the parameters considered, variation in surface density of glial transporters had the largest effect on glutamate concentrations. The stochastic diffusion model of the example synapse was further generalized to characterize glial morphology by studying the role of diffusion path length in supporting neurotransmitter gradients and isolating the synapse. For the same set of parameters, diffusion path length was found to be proportional to the gradient supported.

1 Introduction

A typical chemical synaptic environment has substantial morphological specialization that reflects functional requirements in controlling the movement of substances. The glial environment is a critical regulator of communication and cross-talk between synapses (Barbour, 2001; Rusakov, 2001; Franks, Bartol, & Sejnowski, 2002; Savtchenko & Rusakov, 2007; Zheng, Scimemi, & Rusakov, 2008), and probably of the overall extrasynaptic transmission in the central nervous system (Bergles & Jahr, 1997; Danbolt, 2001). Besides the structure of the perisynaptic glial environment, a number of mechanisms participate in the synaptic tuning of circuits in brain tissue that contribute to synaptic efficacy, plasticity, and neurotransmitter homeostasis in the extracellular space (ECS; Zheng et al., 2008). These mechanisms include vesicular release, neurotransmitter diffusion into the perisynapse, receptor activity (e.g., AMPA and NMDA), inhibition of synaptic vesicular release via activation of negative feedback autoreceptors (e.g., mGluR2/3), binding to and uptake by glial transporters, and nonsynaptic neurotransmitter production (e.g., via cystine-glutamate exchange located primarily on glia). However, the specifics of how the glial environment and the various mechanisms involved achieve neurotransmitter homeostasis are not completely understood. Further, the presence of multiple interacting parameters makes it difficult to achieve precise experimental control near a single synapse. Therefore, an alternative is to construct a computational model to study the role of glial morphology and associated mechanisms in shaping the neurotransmitter landscape and receptor activity.

Previous modeling studies related to neurotransmitter time courses (e.g., glutamate) have focused on synaptic receptor activation (Clements et al., 1992; Franks et al., 2002) and have determined the accessibility of synaptically released neurotransmitter to the ECS by considering diffusion out of the synapse and elimination by glial transporters (Barbour, 2001; Diamond, 2005). These neurotransmitter diffusion models have relied on simple geometric representations of ECS and were based on analytical (Holmes, 1995; Kleinle et al., 1996), continuum (Rusakov & Kullmann, 1998; Rusakov, 2001) or stochastic approaches (Clements, 1996; Stiles, Van Helden, Bartol, Salpeter, & Salpeter, 1996; Franks et al., 2002; Tao & Nicholson, 2004; Savtchenko & Rusakov, 2007; Zheng et al., 2008).

Chronic cocaine administration causes instability of extracellular glutamate levels in the nucleus accumbens, a brain nucleus critical for cocaine reward and relapse (Koob & Le Moal, 2001; Kalivas, Volkow, & Seamans, 2005). A failure of the prefrontal cortex to control drug-seeking behaviors can be linked to an enduring imbalance between synaptic and nonsynaptic glutamate, termed glutamate homeostasis, and this imbalance engenders changes in neuroplasticity that impair communication between the

prefrontal cortex and the nucleus accumbens (Kalivas, 2009). Further, after withdrawal from cocaine, extrasynaptic glutamate levels are reduced in the nucleus accumbens due to downregulation of cystine-glutamate exchange (Baker et al., 2003; Kau et al., 2008). As well, during cocaine relapse, the release of synaptic glutamate in cortico-accumbens synapse is augmented due to reduced tone by extracellular glutamate on release regulating presynaptic metabotropic glutamate receptors (Moran, McFarland, Melendez, Kalivas, & Seamans, 2005) and due to impaired elimination of extracellular glutamate via a reduction in glutamate uptake into the glia (Knackstedt, Melendez, & Kalivas, 2010). Pendyam, Mohan, Kalivas, and Nair (2009) reported a compartmental model of the synaptic environment based on a continuum approach that successfully modeled the cocaine-induced neuropathology at glutamatergic synapses on accumbens spiny neurons. By incorporating cystine-glutamate exchanger as a nonsynaptic release site for glutamate, they showed how cocaine-induced neuroadaptations influence glutamate transmission at accumbens glutamatergic synapses and predicted the subsequently discovered cocaine-induced downregulation of the glial glutamate transporter (Knackstedt et al., 2010). We extended the compartmental model used in Pendyam et al. (2009) in this study to provide molecular-level details of neurotransmitter homeostasis that could not be predicted by alternative models based on continuum approaches. This was done by developing a three-dimensional stochastic diffusion model of a cortico-accumbens synapse (see Figure 1). The molecular diffusion model considered a realistic morphological representation of glia and ECS. The model was then generalized to quantify the role of diffusion path length (defined as the distance that a molecule travels from the synaptic cleft to the ECS) in supporting neurotransmitter gradients by considering several candidate glial configurations.

2 Methods

An example case of a cortico-accumbens synapse was used to illustrate the proposed computational framework. The molecular diffusion model was constrained using biological data, including known parameter ranges (see Table 1).

2.1 Model Inputs.

2.1.1 Firing Frequency and Molecules per Release. For the glutamatergic cortico-accumbens synapse example case, basal presynaptic firing frequency ranged from 1 Hz to 3 Hz (Trantham, Szumlinski, McFarland, Kalivas, & Lavin, 2002), with burst frequencies up to 15 Hz during natural reward-seeking behavioral states (Chang, Zhang, Janak, & Woodward, 1997; Sun & Rebec, 2006). Neurotransmitter release from a nerve terminal

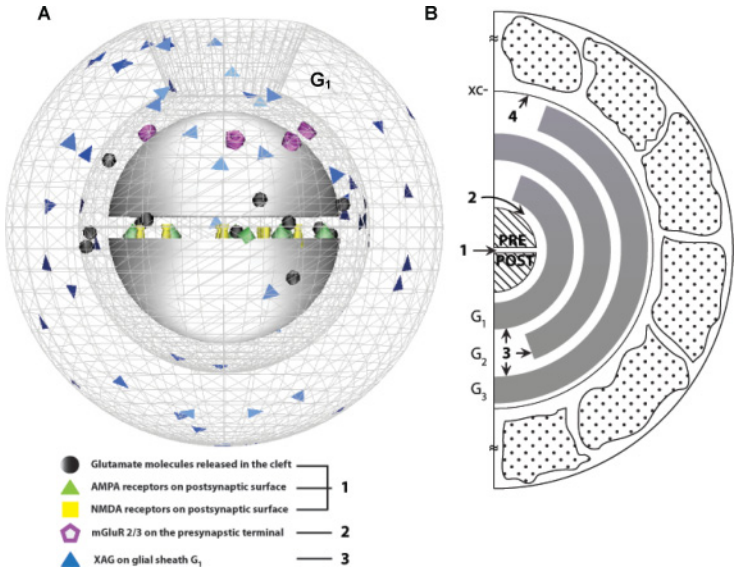

Figure 1: (A) A three-dimensional representation of the cortico-accumbens synapse. Glutamate molecules diffuse across the synaptic cleft (height: 30 nm) separating the two hemispheres of radius $r = 160$ nm. The postsynaptic surfaces were populated with ionotropic receptors (AMPA and NMDA). The metabotropic glutamate receptors (mGluR2/3) were located at $\varphi = 20^{\circ}$ around the presynaptic terminal, with glutamate transporters (XAG), populated on the glial sheath surface (G_1). The impermeable glial sheath G_1 is represented as a wire-frame mesh with an opening on the top. The other glial sheaths, G_2 and G_3, are oriented as shown in panel B. The 3D model was rendered using DReAMM software. (B) Two-dimensional representation of the 3D cortico-accumbens synapse used to study glutamate homeostasis. The synapse was surrounded by glial sheaths (G_i, $i = 1$–3; $i = 1$ being the closest to the synapse) with the highest density of XAG in G_1. Diffusion path length was defined as the distance that a molecule travels from the synaptic cleft to the ECS (i.e., from the center of the synaptic cleft to the G_3 opening). Each glial sheath was 100 nm thick, with binding, uptake, and efflux modeled as stochastic processes. Cystine-glutamate exchanger (xc-) was incorporated as the nonsynaptic release site for glutamate and modeled on the outer surface of glial sheath G_3. The complex structural geometry in the porous ECS consisted of glial boulders randomly placed in the porous neuropil to yield experimental estimates of volume fraction. $[Glu]_{syn}$, $[Glu]_{mGluR}$, and $[Glu]_{ex}$ represented glutamate concentrations measured within the synaptic cleft, near mGluR2/3 and extracellular space beyond glial sheath G_3 respectively. The numbers labeled represent the location of the molecular reactions: (1) ionotropic receptor reactions (see equations 2.1A and B), (2) metabotropic receptor reactions (see equation 2.2), (3) glial XAG reactions (see equations 2.3 and 2.4), and (4) nonsynaptic glutamate (xc-, see equation 2.5).

Table 1: Ranges of Parameter Values for the Example Case Cortico-Accumbens Synapse in Figure 1.

Parameter	Model Value[a]	Range of Values (Citation)
Diffusion coefficient (μm^2/ms)	0.085	0.05–0.75 (Rusakov & Kullmann, 1998; Saftenku, 2005)
xc- (mM hr^{-1})	17 [b]	5–50 (Baker et al., 2003)
AMPA/NMDA dynamics		
AMPA		
k_{C0C1}/k_{C1C0}, ($M^{-1}s^{-1}$)/(s^{-1})	4.59×10^6 /4.26×10^3 ,	(Jonas, Major, & Sakmann, 1993; Franks et al., 2002; Attwell & Gibb, 2005)
k_{C1C2}/k_{C2C1}, ($M^{-1}s^{-1}$)/ (s^{-1})	2.84×10^3 /3.26×10^3 ,	
k_{C2O}/k_{OC2}, (s^{-1})/ (s^{-1})	4.24×10^3 /900,	
k_{C1C3}/k_{C3C1}, (s^{-1})/(s^{-1})	2.89×10^3 /39.2,	
k_{C3C4}/k_{C4C3}, ($M^{-1}s^{-1}$)/(s^{-1})	1.27×10^6/45.7,	
k_{C2C4}/k_{C4C2}, (s^{-1})/(s^{-1})	172/0.727,	
k_{C4C5}/k_{C5C4}, (s^{-1})/ (s^{-1})	16.8/190.4,	
k_{OC5}/k_{C5O} (s^{-1})/ (s^{-1})	17.7/4.0	
NMDA		
k_{C0C1}/k_{C1C0}, ($M^{-1}s^{-1}$)/(s^{-1})	$2.0 \times 5.0 \times 10^6$/4.7,	(Lester & Jahr, 1992; Franks et al., 2002; Attwell & Gibb, 2005)
k_{C1C2}/k_{C2C1}, ($M^{-1}s^{-1}$)/(s^{-1})	5.0×10^6/2.0×4.7,	
k_{C2O}/ k_{OC2}, (s^{-1})/ (s^{-1})	46.5/91.6,	
k_{C2C3}/k_{C3C2} (s^{-1})/(s^{-1})	8.4/1.8	

Table 1: *(Continued.)*

Parameter	Model Value[a]	Range of Values (Citation)
Transporter dynamics		
XAG (molecules/μm^2)	[c]	2,500–10,000 (Bergles & Jahr, 1997; Lehre & Danbolt, 1998)
k_1 ($M^{-1}\,ms^{-1}$)/ k_{-1} (ms^{-1})/k_2 (ms^{-1})	10^4/0.2/0.1	10^4 /0.2/0.1(Lehre & Rusakov, 2002)
Release parameters		
Number of molecules per release	22,000	4,700–80,000 (Bruns & Jahn, 1995)
K_d value of mGluR2/3 (μM)	0.187	0.1–0.3 (Schoepp & True, 1992)
Maximum release probability	0.4 (max)	0.1–0.5 (Billups, Graham, Wong, & Forsythe, 2005; Volynski, Rusakov, & Kullmann, 2006)
Release probability used (tuned to operate near K_d value of mGluR)	0.12 (basal)	(based on log-linear interpolation from values citied in Xi, Baker, Shen, Carson, & Kalivas, 2002)
Presynaptic firing frequencies		
Firing frequency (Hz; basal)	1–2	1–3 (Trantham, Szumlinski, McFarland, Kalivas, & Lavin, 2002)
Firing frequency (Hz; natural reward seeking)	12–15	12–15 (Chang, Zhang, Janak, & Woodward, 1997; Sun & Rebec, 2006)
Geometric parameters		
Average extracellular gap (nm)	40	34–68 (Thorne & Nicholson, 2006)
Intersynaptic distance (μm)	2	2–20 (Rusakov, 2001)

[a]Values used to populate the configuration in Figure 1.
[b]Surface density (molecules/μm^2) of xc- was distributed on the outer surface of the glial sheath,
G_3 as follows for the control cases: 111; corresponding molecules of xc—471.
[c]Surface density (molecules/μm^2) of XAG was distributed as follows for the control cases: G_1—1700, G_2—400, and G_3—400; corresponding molecules of XAG: G_1—2771, G_2—1490, and G_3—2708.

during exocytosis depends on the size of the synapse; vesicular properties such as volume, neurotransmitter concentration, and number available; and geometric parameters such as diameter of the fusion pore (Danbolt, 2001). For general synapses, molecules per release typically vary from 4,000 to 80,000 (Bruns & Jahn, 1995), and this was the range used in the study (see Table 1).

2.1.2 Autoreceptor Regulation of Release Probability. Release probability is regulated following the stimulation of presynaptic autoreceptors (e.g., mGluR2/3–glutamate; Billups, Graham, Wong, & Forsythe, 2005), which are located outside the synaptic cleft (Alagarsamy, Sorensen, & Conn, 2001). The probability that an action potential results in a vesicular release ranges from <0.1 to 1 (Murthy & Sejnowski, 1997). For the example case considered, GTPγS binding revealed that G protein signaling by stimulating mGluR2/3 increased as a logarithm of agonist dose (Xi et al., 2002); hence, the relationship between release probability and percentage occupancy of autoreceptors was assumed to be logarithmic. Percentage occupancy was defined as the ratio of the number of mGluR2/3 activated by the diffusing glutamate molecules in the model to the total number of mGluR2/3 present. Using the relationship between release probability and percentage occupancy, the mGluR2/3 autoreceptor function was modeled as a change in release probability from 0.12 (basal) to 0.10 (natural reward seeking; see Table 1). The release probability was iteratively determined to satisfy model constraints, as discussed later. Thus, each action potential in the model resulted in an instantaneous release of molecules into the cleft. For example, a firing frequency of 2 Hz had a release probability of 0.12 in the control basal case, and, on average, it resulted in a release event every 4.17 seconds.

2.1.3 Ionotropic Receptors. Synaptic receptors (AMPA and NMDA) were co-localized in the cleft with an AMPA/NMDA ratio of 0.81 ± 0.33 ($n = 17$; mean $\pm$ sd; unpublished data) based on the maximum peak height of the current obtained during basal conditions in the nucleus accumbens. This was in the range of previous reports that measured AMPA/NMDA ratio in accumbens brain slices (Thomas, Beurrier, Bonci, & Malenka, 2001; Wolf et al., 2005; Kourrich, Rothwell, Klug, & Thomas, 2007; Conrad et al., 2008).

2.1.4 Diffusion. Diffusion of neurotransmitter in the ECS is complicated by several factors, such as glial geometry, receptor binding, transporter uptake, viscosity, temperature, change in structure with time (Nicholson, 2001; Franks et al., 2002; Hrabe, Harbetova, & Segeth, 2004; Sykova, 2004; Diamond, 2005; Saftenku, 2005), and change in local properties with pathology (e.g., volume fraction; Sykova, 1997). Diffusion in the porous neuropil is typically characterized by volume fraction α (void space/total tissue volume) and tortuosity λ (hindrance to diffusion imposed by local boundaries

or local viscosity; Nicholson, 2001). Volume fraction α in brain tissue is estimated to be around 0.2 (Nicholson & Sykova, 1998) while tortuosity λ is estimated to be in the range 1.2 to 2.4 based on diffusion measurements over a distance of 100 μm to 300 μm (Nicholson, 2001). However, experimental estimates of diffusion coefficients (D) in the perisynaptic region ($<1\,\mu$m from cleft) have not been reported for synapses with tightly packed glia (Rusakov & Kullmann, 1998; Hrabe et al., 2004). Hence, in the proposed model D was iteratively determined in the range, 0.05 $\mu m^2/ms$ to 0.41 $\mu m^2/ms$ (Saftenku, 2005; see Table 1) to satisfy model constraints described later.

2.1.5 Glutamate Transporters. Glial transporters (XAG) modulate glutamate transmission by regulating neurotransmitter access to glutamate receptors and to ECS, thus maintaining appropriate neurotransmitter gradients (Danbolt, 2001; Zheng et al., 2008; Pendyam et al., 2009). XAG present on glial membranes (Danbolt, 2001) have surface densities ranging from 2,500 to 10,000 molecules/μm^2 (Bergles & Jahr, 1997; Lehre & Danbolt, 1998). For the model examined here, equivalent surface density of XAG was determined iteratively within the cited range to satisfy the model constraints listed in Table 2.

2.1.6 Cystine-Glutamate Exchanger. Estimated extracellular concentrations of glutamate can vary from 25 nM (Herman & Jahr, 2007) to 5 μM (Baker et al., 2003). In vivo extrasynaptic concentrations assessed by microdialysis revealed that the majority of glutamate outside the synaptic cleft is not of synaptic origin (Timmerman & Westerink, 1997; Melendez, Vuthiganon, & Kalivas, 2005). Also, extracellular glutamate in tissue slices and cell culture experiments is partly of nonsynaptic origin (Haydon, 2001; Le Meur, Galante, Anulo, & Audinat, 2007). While a number of sources of nonsynaptic extracellular glutamate have been suggested (Danbolt, 2001; Haydon, 2001; Baker et al., 2003; Cavelier, Hamann, Rossi, Mobbs, & Attwell, 2005), extracellular glutamate measured by microdialysis in the accumbens arises primarily from cystine-glutamate exchange (xc-; Xi et al., 2002; Baker et al., 2003). The production rate of xc- was in the range of 5–50 mM hr^{-1} (also see Pendyam et al., 2009) and was estimated iteratively by varying the surface density of xc- on glia to satisfy model constraints, as discussed later (see Table 1).

2.2 Cocaine-Induced Neuroadaptations. Chronic cocaine administration causes instability in extracellular glutamate in the nucleus accumbens, a brain nucleus critical for cocaine reward and relapse (Koob & Le Moal, 2001; Kalivas et al., 2005). Rats withdrawn from chronic cocaine administration show dysregulation of extracellular glutamate in the nucleus accumbens due in part to reduced xc- and mGluR2/3 signaling (Baker et al., 2003). Microdialysis measurements during drug-seeking conditions have

Table 2: Steady-State Neurotransmitter Concentration Constraints for the Example Case Cortico-Accumbens Synapse.

	Control		Cocaine	
Parameter (μM)	Basal	Natural Rewards	Basal	Drug Seeking
$[Glu]_{syn}$	0.1 (Patneau & Mayer, 1990)	0.1 (Patneau & Mayer, 1990)	-	-
$[Glu]_{mGluR}$	0.1–0.3 (Schoepp & True, 1992)	0.1–0.3 (Schoepp & True, 1992)	-	-
$[Glu]_{ex}$	5.6 ± 1.0 (Baker et al., 2003)	5.6 ± 1.0	2.89 ± 0.34 (Baker et al., 2003)	13.3 ± 1.4 (Szumlinski et al., 2006; McFarland, Lapish & Kalivas, 2003; McFarland, Davidge, Lapish, & Kalivas, 2004)
Model estimates at varying firing frequencies using control and cocaine parameters averaged across 10 trials				
$[Glu]_{syn}$	0.16	0.19	0.28	1.33
$[Glu]_{mGluR}$	0.21	0.22	0.32	1.51
$[Glu]_{ex}$	4.79 ± 0.04	5.32 ± 0.06	3.29 ± 0.04	12.50 ± 0.05

shown a significant overflow of synaptic glutamate (McFarland et al., 2003, 2004). Other changes included alterations in the following: glutamate release (McFarland et al., 2003), postsynaptic glutamate signaling (Conrad et al., 2008), group II metabotropic glutamate receptors (mGluR2/3; Xi et al., 2002), and AMPA/NMDA ratio. Based on these experimental findings, xc- production was reduced by 50%, the mGluR2/3 autoreceptor function was modeled as a change in release probability from 0.32 (cocaine basal) to 0.30 (cocaine drug seeking), and the AMPA/NMDA ratio was changed to 1.15 ± 0.41 ($n = 12$; unpublished data). By incorporating cystine-glutamate exchange as a nonsynaptic release site for glutamate, Pendyam et al. (2009) were able to show how cocaine-induced neuroadaptations influence glutamate transmission at accumbens glutamatergic synapses and predicted the subsequently discovered cocaine-induced downregulation of the glial glutamate transporter (Knackstedt et al., 2010). The stochastic approach was also employed to verify this finding.

2.3 Development of the Stochastic Model. The stochastic molecular diffusion model was created using the MCell program (version 3.1.812), a general Monte Carlo simulator designed for cellular microphysiology studies (Stiles et al., 1996; Stiles & Bartol, 2001; Kerr et al., 2008). A three-dimensional spatially realistic model of the cortico-accumbens synapse was constructed using the software Blender (www.blender.org), an open source modeling and animation package that can export model description language (MDL) files to MCell. The MDL files are used to specify the types of molecules in the model, their diffusion constants, initial locations, reactions, and stoichiometry (Czech, Dittrich, & Stiles, 2009). To facilitate visual rendering and checking by animating simulation, MCell exports mesh objects, molecules, and receptor site positions and their states to the DReAMM program (www.mcell.psc.edu) in a suitable format, with molecule positions recorded at every time step. This requires PSC DX, which is derived from OpenDX but improved in several aspects. The model developed in MCell allows the integration of mechanisms, kinetics, and stochastic behaviors at the molecular level, with structural organization and function at the cellular level.

The representative model geometry was built in silico with meshes (geometric surfaces) being reflective to diffusing molecules. Meshes that were populated with different types of surface molecules (e.g., mGluR2/3, XAG) were first triangulated, and each element was tiled using barycentric subdivision. A large number of bimolecular reactions were defined with associated rate constants to investigate receptor occupancy and opening, uptake, and neurotransmitter homeostasis.

The geometry of the example case cortico-accumbens (see Figure 1) consisted of a synapse surrounded by assemblies of simplified glial sheaths (G_i) with porous space between them (Rusakov, 2001) as observed in vivo (Rusakov & Kullmann, 1998). The configuration in Figure 1 was modeled

with an average porous gap of 40 nm (Thorne & Nicholson, 2006) between the impermeable glial sheaths ($G_{1\text{-}3}$). Each glial sheath was 100 nm thick (Rusakov, 2001) based on the minimum width of glial profiles observed in electron micrograph studies. The structure of an individual glial sheath was akin to that previously reported (Rusakov, 2001; Pendyam et al., 2009) but the multiple sheaths ($G_{1\text{-}3}$) were configured iteratively to satisfy the model constraints listed in Table 2. The postsynaptic surfaces of the synaptic cleft (height: 30 nm) were populated with ionotropic receptors (AMPA and NMDA). The metabotropic glutamate receptors (mGluR2/3) were located at $\varphi = 20^{\circ}$ around the presynaptic terminal, and the glial glutamate transporters, XAG, were distributed on the glial sheath surface ($G_{1\text{-}3}$; see Figure 1). Based on studies indicating that the highest densities of XAG were closer to the synapse (Danbolt, 2001; Lehre & Danbolt, 1998), G_1 had the highest surface density of XAG (see Table 1). The nonsynaptic release sites for glutamate, namely, cystine-glutamate exchanger, xc-, were modeled as being located on the outer surface of the glial sheath G_3. Beyond G_3, the porous ECS contained randomly placed glial boulders of varying dimensions without surface-populated XAG or xc-. The configurations of the glial sheaths and boulders in the model were iteratively varied to obtain a volume fraction of approximately 0.23 (Sykova, 2004). Further, the total number of spines along the length of the dendritic segment was found to be approximately 10 spines/10 μm (Robinson & Kolb, 1999). Assuming that 50% of these had projections from the prefrontal cortex (PFC), each synapse could have an average intersynaptic distance of 1 μm. Thus, a no-flux boundary condition was imposed at the outer edge of the model (approximately 1 μm from the edge of the synapse) such that no molecules entered or left the outer boundary and thus simulated identical neighboring synapses.

Tortuosity is a composite parameter that contains a significant geometrical component, although other factors such as interstitial viscosity may contribute (Tao, Tao, & Nicholson, 2005). However, in the MCell simulator, the geometric and viscous components of tortuosity are not combined. A lower diffusion coefficient than water ($<1\ \mu m^2/ms$) is attributed to the microscopic viscous drag on the diffusing molecule at atomically fine spatial scales. This would include the molecule interactions with the proteins and microfilaments in the ECS. The additional interactions that the molecules have with larger-scale diffusion barriers such as spines, small axonal boutons, and glia fall under geometric tortuosity. This is not accounted for in the diffusion coefficient, D. Hence, to compute the geometric tortuosity, we performed experiments with a point source as outlined in Tao and Nicholson (2004). This required the elimination of all the reactions that the diffusing molecules have with receptors and transporters, that is, all such reactions were turned off. The estimated effective diffusion constant was approximately 10 times smaller than the microscopic D value for the glutamate molecule. This resulted in a tortuosity value of 3.16 for the configuration in Figure 1.

Concentration within the synaptic cleft (of volume $2.29 \times 10^{-3}\ \mu m^3$) represented as $[Glu]_{syn}$ and near mGluR2/3 (located at $\varphi = 20^\circ$ with a volume $1.25 \times 10^{-4}\ \mu m^3$) represented as $[Glu]_{mGluR}$, were computed using the total number of free glutamate molecules in the respective regions after reaching homeostasis. The experimentally defined concentrations of glutamate in the extracellular space (ECS of volume $1.418\ \mu m^3$), represented as $[Glu]_{ex}$ and reported by in vivo microdialysis (Baker et al., 2003; McFarland et al., 2003, 2004; Szumlinski et al., 2006) during control and cocaine conditions, were modeled as being outside glial sheath G_3. After the transient phase (i.e., 50 ms after a synaptic release), the concentration stabilized, leading to a uniform profile and thus homeostatic $[Glu]_{syn}$, $[Glu]_{mGluR}$, and $[Glu]_{ex}$ were spatially averaged in the respective regions for 1000 ms for the control and cocaine cases.

Thus, on release from the center of the synapse, glutamate molecules diffused across the synaptic cleft to activate ionotropic receptors on the postsynaptic terminal. Uptake of diffusing molecules outside the cleft occurred by molecular reactions with surface-populated glutamate transporters located on the glial surfaces. Details related to the implementation of diffusion-reaction systems on surfaces and in a solution used by MCell can be found in Kerr et al. (2008).

2.4 Implementation of the Kinetics and Reaction Schemes. The diffusing glutamate molecules stochastically interacted with the surface-populated receptors (AMPA, NMDA, mGluR2/3, and XAG) based on the reaction schemes described in Franks et al. (2002) and Rusakov (2001). On release, glutamate molecules reacted with synaptic receptors (e.g., AMPA and NMDA) following the kinetic schemes in equations 2.1 A and 2.1B, respectively:

$$\begin{array}{ccccccc} C0 + [Glu] \underset{K_{C1C0}}{\overset{K_{C0C1}}{\leftrightarrow}} & C1 & + [Glu] \underset{K_{C2C1}}{\overset{K_{C1C2}}{\leftrightarrow}} & C2 & \underset{K_{0C2}}{\overset{K_{C20}}{\leftrightarrow}} & O, \\ & K_{C3C1} \updownarrow K_{C1C3} & & K_{C4C2} \updownarrow K_{C2C4} & & K_{C5O} \updownarrow K_{OC5} \\ & C3 & + [Glu] \underset{K_{C4C3}}{\overset{K_{C3C4}}{\leftrightarrow}} & C4 & \underset{K_{C5C4}}{\overset{K_{C4C5}}{\leftrightarrow}} & C5 \end{array} \tag{2.1A}$$

$$\begin{array}{ccccc} C0 + [Glu] \underset{K_{C1C0}}{\overset{K_{C0C1}}{\leftrightarrow}} & C1 + [Glu] \underset{K_{C2C1}}{\overset{K_{C1C2}}{\leftrightarrow}} & C2 & \underset{K_{0C2}}{\overset{K_{C20}}{\leftrightarrow}} & O, \\ & & K_{C3C2} \updownarrow K_{C2C3} & & \\ & & C3 & & \end{array} \tag{2.1B}$$

where all receptors were in state C0 (closed state) before release. Upon binding with molecules of glutamate [*Glu*], the receptors changed states as shown. C1 and C2 correspond to the single- and double-liganded closed states, respectively, with C3, C4, and C5 representing the other intermediate states and O representing the open state of the receptor. The rate constants describing the AMPA and NMDA receptor kinetics were adapted from

Franks et al. (2002), who based it on previously published work by Jonas et al. (1993) for AMPA and Lester and Jahr (1992) for NMDA (see Table 1).

The kinetic scheme for the mGluR2/3 binding to diffusing glutamate was given by equation 2.2,

$$[Glu] + [R] \underset{k_{-1}}{\overset{k_1}{\Leftrightarrow}} [GluR], \tag{2.2}$$

where [*Glu*], [*R*], and [*GluR*] represented the molecules of glutamate, metabotropic glutamate receptors (mGluR2/3), and the glutamate-receptor bound complex, respectively. Unlike AMPA and NMDA, due to the lack of experimental data, the binding kinetics for mGluR2/3 of $k_1 = 10^5$ M^{-1} ms^{-1} and $k_{-1} = 18 \times 10^{-3}$ ms^{-1} were iteratively determined based on the disassociation constant K_d (~0.187 nM; Schoepp & True, 1992) to satisfy nominal values of glutamate concentration near mGluR2/3 and to simultaneously achieve approximately 85% mGluR2/3 occupancy in order to establish autoreceptor tone during control basal conditions.

The surface-populated XAG on the glial sheaths $G_{1\text{-}3}$ interacted with the diffusing glutamate molecules as per the reaction scheme in

$$[Glu] + [XAG] \underset{k_{-1}}{\overset{k_1}{\Leftrightarrow}} [Glu - XAG] \overset{k_2}{\Rightarrow} [Glu_{in}] + [XAG], \tag{2.3}$$

where [*XAG*] and [*Glu–XAG*] represented the glial glutamate transporters, and the glutamate-transporter complex, respectively, and [Glu_{in}] represented the uptake of glutamate by XAG. The kinetics for XAG of $k_1 = 10^4$ M^{-1} ms^{-1}, $k_{-1} = 0.2$ ms^{-1}, and $k_2 = 0.1$ ms^{-1} were taken from Rusakov (2001) who based it on experiments by others (Wadiche, Arriza, Amara, & Kavanaugh, 1995; Bergles & Jahr, 1997). [*GluD*] represented the glutamate removed from the system in the glia and was given by equation (2.4), with a rate $k_3 = 0.026$ ms^{-1} (Geiger, Roth, Taskin, & Jonas, 1999):

$$[Glu_{in}] \overset{k_3}{\Rightarrow} [GluD]. \tag{2.4}$$

The glial surfaces were modeled as being reflective to diffusing molecules with no intracellular diffusion mechanism modeled within the glia.

Cystine-glutamate exchanger, xc-, was incorporated as the nonsynaptic release source for glutamate and was modeled outside glial sheath G_3. The kinetic scheme for xc- to release glutamate molecules into the ECS of volume 1.418 μm^3 was given by

$$[CG] \overset{k_4}{\Rightarrow} [Glu], \tag{2.5}$$

where [CG] represented the cystine-glutamate exchanger, xc-, producing glutamate at the rate $k_4 = 0.092$ ms^{-1} (17 mM hr^{-1}; Pendyam et al., 2009).

2.4.1 Iterative Evaluation. The iterative process began with values in the lower end of the ranges for the parameters (for, e.g., number of molecules, D, XAG and xc- surface density) reported in Table 1, while monitoring $[Glu]_{syn}$, $[Glu]_{mGluR}$, $[Glu]_{ex}$ and mGluR2/3 occupancy. As part of the iterative process, we compared mGluR2/3 occupancy and the release probability used to check if they satisfied the log-linear function; if not, the release probability was adjusted. Once determined for a particular case, there was no change in release probability during the simulations or between release events. After satisfying the requirements for the control cases, the cocaine basal and cocaine-seeking cases were simulated by modeling known cocaine-induced changes to xc- (modeled by reducing total number of xc- molecules by 50%), mGluR2/3 signaling (modeled by changing the release probability for cocaine cases in the range 0.32–0.30), and AMPA/NMDA ratio (modeled by increasing the AMPA receptors to 29 from 18 in the control cases). The changes observed in the $[Glu]_{ex}$ during cocaine pathologies did not occur in the stochastic model until the 40% cocaine-induced downregulation of XAG was incorporated. Thus, the stochastic model validated the downregulation of XAG that was previously predicted (Pendyam et al., 2009) and subsequently discovered experimentally (Knackstead et al., 2010). The model values listed in Table 1 constituted the values that satisfied all the model constraints simultaneously (see Table 2): steady-state $[Glu]_{syn}$, $[Glu]_{mGluR}$, and $[Glu]_{ex}$ in the control basal, natural reward-seeking, cocaine basal, and cocaine-seeking cases while maintaining 85% mGluR2/3 occupancy for the control basal case.

Through further iterative changes, multiple parameter sets were identified that satisfied some of the model constraints in control and cocaine conditions. For example, a wide range of molecular release (e.g., 1000–15,000) satisfied $[Glu]_{ex}$ in the control cases and the cocaine basal case but was insufficient to establish $[Glu]_{ex}$ under the cocaine drug-seeking case. Thus, it was iteratively determined that a release of 22,000 molecules was required during every action potential to satisfy $[Glu]_{ex}$ for the cocaine drug-seeking case. Hence, for consistency 22,000 molecules were chosen per release for all cases considered.

Also, the kinetic values for the Glu-mGluR2/3 reaction (see equation 2.2) chosen in the model did not affect the key ideas presented in this letter. We found that for the configuration in Figure 1, higher values of kinetic constants (for, e.g., $k_1 = 10^8\ M^{-1}\ ms^{-1}$ and $k_{-1} = 18\ ms^{-1}$), although physiologically unrealistic, resulted in a lower mGluR2/3 occupancy ($\sim$50%) without altering glutamate concentrations, indicating that the model was internally consistent.

All simulations were implemented on a Dell EM64 T and SGI Altix 4700 cluster using the Linux operating system. The model used a time step of 0.5 μsec so that the corresponding mean diffusion length computed by MCell allowed the system to be sampled sufficiently at this scale. This was done after ensuring that all reaction probabilities in the model were less than

0.05 to ensure accurate sampling of the diffusing molecules of the system. This also resulted in sufficiently small errors in the reaction equilibria. At the initialization of each simulation, the exact number and position of receptors were randomly assigned by MCell on specified surfaces (e.g., XAG on glial sheath G_1 varied from 2737 to 2874 molecules between trials) based on the average surface densities (see Table 1). Various bound and unbound complexes of the reactions were also tracked to obtain a spatiotemporal estimate of the reactants in the system. Conservation of molecules was confirmed at each time step by computing the numbers of free, bound, and transported glutamate molecules. Due to the stochastic nature of the model, multiple trials were conducted to obtain average estimates for $[Glu]_{syn}$, $[Glu]_{mGluR}$, and $[Glu]_{ex}$. The model was simulated for 6 seconds so as to achieve homeostatic conditions for each of the cases considered (control basal, control rewards, cocaine basal, and cocaine seeking).

The surface density values for the receptors used in the model were determined by averaging over 48 trials after ensuring that the steady-state concentrations for $[Glu]_{syn}$, $[Glu]_{mGluR}$, and $[Glu]_{ex}$ were within one standard deviation of the corresponding reported experimental means. We then used the average value obtained for the receptors (AMPA, NMDA, mGluR2/3, XAG, and xc-) based on the surface density from the 48 trials and ran 10 additional trials for all the cases. That is, we kept the input parameter numbers constant in MCell for the 10 trials to estimate average values for $[Glu]_{syn}$, $[Glu]_{mGluR}$, and $[Glu]_{ex}$. As expected, the concentration estimates for these 10 runs were also within one standard deviation from the experimentally reported mean for all cases considered. Thus, all results reported in this letter were across 10 simulations.To check for numerical accuracy, we decreased the time step by a factor of 5, and no significant changes ($\sim$3%) were found in $[Glu]_{syn}$, $[Glu]_{mGluR}$, and $[Glu]_{ex}$. Tables 1 and 3 list the surface density and number of receptor molecules (AMPA, NMDA, mGluR2/3, XAG, and xc-) used for the configuration in Figure 1.

3 Results

Multiple 3D configurations of glia surrounding the example case cortico-accumbens synapse were studied by varying the number of glial sheaths, coverage, thickness, and glial boulders in the ECS. As cited above, the input parameters were iteratively adjusted to satisfy model constraints (see Table 2), and by providing appropriate resistance to the flow of glutamate molecules, the configuration in Figure 1 established all model constraints simultaneously.

3.1 Transient and Steady-State Concentration Characteristics. Each synaptic release in the model resulted in peak cleft concentration in the mM range that decayed in a biphasic manner with fast and slow time constants

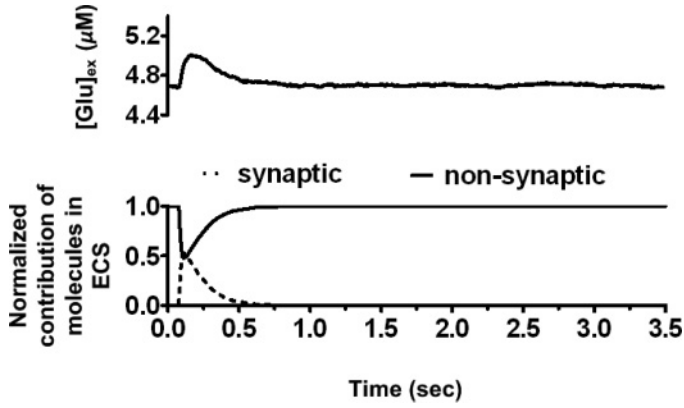

Figure 2: Extracellular glutamate concentration ($[Glu]_{ex}$) in the control basal case and the normalized contribution of glutamate molecules from synaptic and nonsynaptic sources in extracellular space (ECS). By including the cystine-glutamate exchange (xc-) as a nonsynaptic release site for glutamate, the model showed that extracellular concentration was primarily due to the xc- at steady state for the control basal case. This is because the synaptically released glutamate molecules were entirely consumed by transporters located on the glial folds. This study also validated that a wide range of molecular release (e.g., 1000–22,000) could be used to satisfy $[Glu]_{ex}$ in control conditions.

of 85 μs and 3.3 ms, respectively. Further, varying the no-flux boundary condition had no effect on the time course of neurotransmitter in the cleft.

A single glutamate molecule in the synaptic cleft (volume of 2.29×10^{-3} μm^3) resulted in $[Glu]_{syn}$ increasing to approximately 0.7 μM. Since the steady-state biological $[Glu]_{syn}$ were typically three to four times lower (approximately 0.2 μM; Patneau & Mayer, 1990), we concluded that experimental estimates of low steady-state concentrations measured in the synapse may be due to the intermittent presence of a single glutamate molecule. This held true for the region in the vicinity of mGluR2/3 autoreceptors (volume of 1.25×10^{-4} μm^3) where $[Glu]_{mGluR}$ was monitored. By labeling glutamate molecules from synaptic and nonsynaptic sources, the model showed that while transient characteristics were primarily dominated by synaptic release, steady-state concentrations were controlled by the nonsynaptic release site for glutamate—namely, cystine-glutamate exchanger. The relative contributions (normalized) of synaptic and nonsynaptic sources to transient and steady-state glutamate concentrations in the control basal case after a release are shown in Figure 2. Approximately 4250 glutamate molecules of nonsynaptic origin maintained a steady state $[Glu]_{ex}$ of 5 μM in the ECS (volume of 1.41 μm^3) of the configuration in Figure 1. The neurotransmitter molecule numbers in ECS varied from 3750 to 4250 in the control basal case

across 10 trials, resulting in average $[Glu]_{ex}$ being 4.79 $\pm$ 0.04 μM, while average $[Glu]_{ex}$ during the natural reward-seeking case was 5.32 $\pm$ 0.06 μM, corresponding to a molecular variation of 4500 to 5250 across 10 trials. The model reproduced extracellular glutamate concentration levels for cocaine basal and cocaine-seeking cases as 3.29 $\pm$ 0.05 μM and 12.5 $\pm$ 0.06 μM, respectively, only after a 40% reduction in XAG (Knackstedt et al., 2010), verifying the prediction based on a continuum model in Pendyam et al. (2009). This corresponded to a variation of 2500 to 3250 glutamate molecules in the cocaine basal case and 11,750 to 12,500 in the cocaine-seeking case, across 10 trials. Thus, the homeostatic glutamate concentrations that resulted from the configuration in Figure 1 matched the mean field situation observed experimentally using dialysis studies as reported in Table 2.

3.2 Receptor Opening During Control and Cocaine Conditions. The AMPA/NMDA ratio was 0.8 $\pm$ 0.33 in the control basal case and changed to 1.15 $\pm$ 0.41 ($n = 12$; unpublished data; also see Kourrich et al., 2007; Conrad et al., 2008) in the cocaine basal case in the nucleus accumbens as cited previously. Figure 3 shows the percentage of receptors in the open state for AMPA and NMDA receptors during transient and steady-state conditions for control and cocaine cases in the presence of synaptic and nonsynaptic sources. The percentage of receptors in the open state was defined as the ratio of receptors that reached the open state as modulated by synaptic and nonsynaptic glutamate to the total number of receptors (AMPA or NMDA) in the volume considered. Table 3 shows the surface density and the equivalent number of receptor molecules that were randomly distributed. In the control cases, about 5% of AMPA receptors were in the open state during the transient phase. The AMPA receptors in the open state dropped to about 3% in the cocaine cases despite the total number of AMPA receptors being higher (see Table 3). Although most of the AMPA receptors were activated by synaptically released glutamate, less than 10% reached the open state, with many AMPA receptors existing in one of the intermediate states (data not shown). As observed in Figure 3, steady-state NMDA receptor activity and opening was also mediated by nonsynaptic glutamate sources during control and cocaine basal conditions. Thus, on average in between spike events, glutamate molecules (nonsynaptic origin) from ECS diffused into the cleft, and this resulted in less than 2% of the high-affinity NMDA receptors being in the open state during the homeostatic control basal case (see Table 3). Since AMPA receptors in the open state were less than 1%, the predicted level of NMDA receptors open would not lead to postsynaptic signaling (Parsons, Danysz, & Zieglgansberger, 2005).

3.3 Perturbation Studies. A perturbation analysis was used to rank the following model parameters using the configuration in Figure 1: total transporter molecules, nonsynaptic glutamate molecules, number of molecules/release, diffusion coefficient, and volume fraction. Each

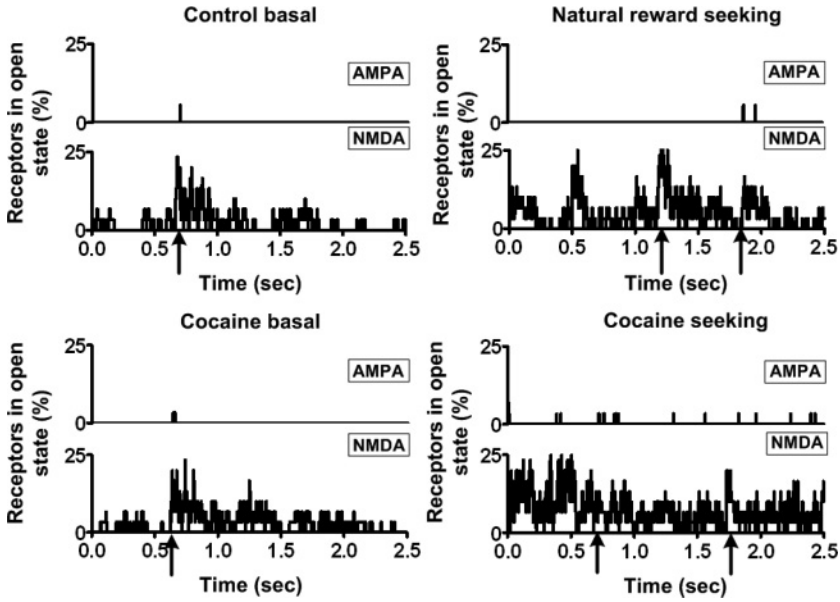

Figure 3: Percentage of AMPA and NMDA receptors in the open state based on synaptic and nonsynaptic neurotransmitter sources. Percentage of receptors in the open state was defined as the ratio of the receptors that are present in the open state to the total receptors present. The arrows are representative of the times at which release occurred in the control basal, natural reward–seeking, cocaine basal, and cocaine-seeking cases with presynaptic firing frequencies: 4.167 Hz, 0.667 Hz, 3.125 Hz, and 0.222 Hz, respectively. On average, in the control conditions, about 5% of AMPA receptors were in the open state during the transient state (immediately after release). The AMPA receptors in the open state, however, dropped to about 3% in the cocaine cases despite the number of AMPA receptors being higher. Also, the steady influx of molecules from the extracellular space to the perisynaptic environment resulted in the high-affinity NMDA receptors being in the open state. In the absence of AMPA-mediated depolarization (<1% in the open state), this would not lead to postsynaptic signaling.

parameter was varied by $+/-10\%$ around the model value in Table 1 to find their relative effect on the steady-state $[\mathrm{Glu}]_{\mathrm{syn}}$ and $[\mathrm{Glu}]_{\mathrm{ex}}$. The differences in the outputs (%) based on this $+/-10\%$ change were then normalized by dividing with the largest value across all parameters. The resulting normalized numbers reported in Table 4 were indicative of the relative importance (rank) of the parameters as far as their effect on the output was concerned. The details of the percentage variation in the parameters of interest compared to the control basal case are reported below.

Table 3: Percentage of Receptors in the Open State (Open Receptor/Total Receptors) During Transient and Steady-State Conditions—For Example, the Cortico-Accumbens Synapse in Figure 1.

Parameter	AMPA	NMDA	mGluR2/3
Total receptors (molecules)	18	30	22
Surface density (molecules/μm^2)	130	200	900
Occupancy in% during transient/steady state			
Control basal[a]	0.05/0	15.39/1.35	84.25/86.84
Control rewards[a]	0.31/0	12.4/2.7	98.1/97.61
Cocaine basal[b]	0.57/0	11.0/1.68	85.7/81.28
Cocaine seeking[b]	0.08/0.07	7.75/4.75	100/99.96

[a]AMPA/NMDA ratio for control case: 0.62 (AMPA receptors = 18; NMDA receptors = 30).
[b]AMPA/NMDA ratio for cocaine case: 0.96 (AMPA receptors = 29; NMDA receptors = 30).
Note: AMPA/NMDA occupancy in transient state averaged for about 50 ms. AMPA/NMDA occupancy in steady state averaged for about 1000 ms.

3.3.1 Total Transporters. A $+/-10\%$ change in XAG on all sheaths G_{1-3} resulted in a change in $[Glu]_{syn}$ by $-25/+37\%$; and in $[Glu]_{ex}$ by $-8/+9\%$. Further, transporters on each glial sheath were varied independently to quantify their role on the outputs of interest. A $+/-10\%$ change in transporters on G_1 alone resulted in a change in $[Glu]_{syn}$ by $-11/+11\%$ and, as expected, resulted in no significant variation in $[Glu]_{ex}$. A $+/-10\%$ change in XAG for G_2 alone resulted in a change in $[Glu]_{syn}$ by $-6/+4\%$ and less than 1% change in $[Glu]_{ex}$. A $+/-10\%$ change in XAG on G_3 alone resulted in a change in $[Glu]_{syn}$ by $-12/+12\%$ and in $[Glu]_{ex}$ by $-7/+8\%$. This study verified the significant role glial sheath G_3 played in regulating the influx of molecules from the ECS into the perisynapse at steady state, thereby controlling $[Glu]_{syn}$ along with maintaining $[Glu]_{ex.}$

3.3.2 Nonsynaptic Sources. A $+/-10\%$ change in xc- resulted in an change in $[Glu]_{syn}$ by $+12/-3\%$ and in $[Glu]_{ex}$ by $+11/-4\%$. This variation could be attributed to the contribution of nonsynaptic sources in maintaining $[Glu]_{ex.}$ An increase in xc- resulted in an increase in $[Glu]_{ex}$, thereby affecting the molecular influx to the perisyanpse and increasing $[Glu]_{syn}$. This trend was consistent with when xc- is reduced, albeit not linear.

3.3.3 Molecules per Release. A $+/-10\%$ change in the number of molecules per release resulted in no change in $[Glu]_{syn}$ and in less than a 0.5% change in $[Glu]_{ex}$. This showed that synaptically released glutamate was consumed entirely by XAG in the control basal case. This also demonstrated that

facilitation or depression of presynaptic release had a minor influence on extracellular concentrations. Thus, a wide range of molecular release could satisfy all study cases besides cocaine drug-seeking cases.

3.3.4 Diffusion Coefficient, D. A $+/-10\%$ change in diffusion coefficient resulted in an change in $[Glu]_{syn}$ by $+19/-16\%$ and a change in $[Glu]_{ex}$ by $-3/+3\%$. Reducing D restricted efflux of molecules to the ECS after a release, and this increased the availability of molecules to the glial-rich transporters in the perisynaptic environment. At the same time, a lower D constrained the influx of molecules from the ECS to the perisynapse during a steady state. Increasing D resulted in a greater movement of molecules in the perisynaptic environment, thereby significantly increasing $[Glu]_{syn}$.

3.3.5 Volume Fraction, α. To study the effect of volume fraction, an extreme case of no glial boulders in the region outside glial sheath G_3 was considered. This led to a fourfold increase in α from 0.2 to 0.9, which resulted in an increase in $[Glu]_{syn}$ by 17%, and in $[Glu]_{ex}$ by 10%. The absence of glial boulders in the ECS resulted in a drop in uptake by glial sheath G_3, thus increasing $[Glu]_{ex}$ and subsequently affecting $[Glu]_{syn}$. As this study highlights, although the glial boulders lacked XAG, their presence in the model improved the uptake efficiency of XAG present on G_3.

3.4 Characterizing Isolation for a General Synapse Based on Glial Sheath Geometry. Certain synapses are tightly ensheathed by glial processes while others are left open (Sykova, 2004; Rollenhagen & Lubke, 2006). The generalized study considered the following question: Given the same parameter set, how do configurations A to F in Figure 4 compare in maintaining a specific neurotransmitter gradient? To characterize diffusion path length (defined as the distance that a molecule travels from the synaptic cleft to the ECS) and synaptic isolation, the stochastic framework for the example case cortico-accumbens synapse was generalized. This was done by considering a lower $[Glu]_{ex}$ of 1 μM, and comparing three types of glial configurations akin to those previous proposed (e.g., Barbour, 2001; Rusakov, 2001), namely, porous (i.e., no glial sheaths and with transporters distributed uniformly in the perisynaptic region), one, and two glial sheaths (see Figure 4). The key difference between the configurations in Figure 4 was their orientation, coverage, placement, and number of glial sheaths, which resulted in different diffusion path lengths. The two-sheath model with the longest path length (configuration G) was set as the baseline model. For this configuration, the diffusion coefficient and the number of transporter and nonsynaptic molecules were iteratively determined to satisfy the following constraints: $[Glu]_{syn}$ of 0.2 μM while maintaining $[Glu]_{ex}$ of 1 μM to establish a neurotransmitter gradient ($[Glu]_{ex}$-$[Glu]_{syn}$) of 0.8 μM.

Further, due to the variability that existed between the models (A–F), for consistency we constrained the parameters to be the same and thus report

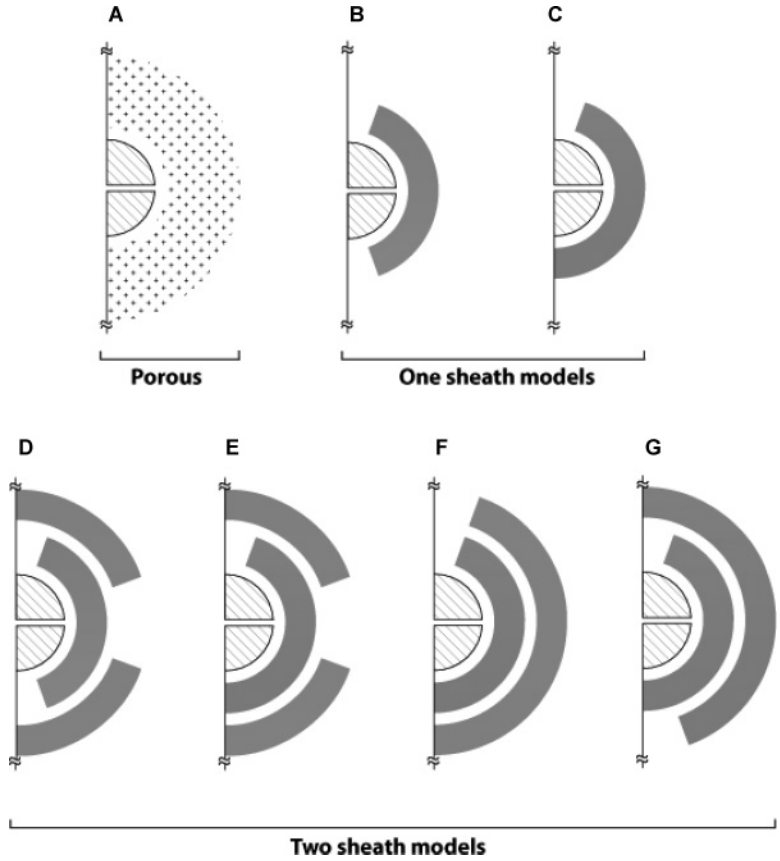

Figure 4: Two-dimensional schematic of the three distinct types of 3D glial configurations (porous, one, and two sheaths) used to characterize diffusion path length and synaptic isolation for a general synapse with 1 μM extracellular concentration, using the same legends as in Figure 1. Glial transporters were randomly distributed in the shaded regions. Configurations B and C with different orientation of glial openings on pre- and postsynaptic regions represent the one-sheath glial cases, and configurations D–G represent two-sheath glial cases considered. The diffusion path length increased from configurations A to G, with configuration G as the baseline model.

the total molecules used. The resulting parameter set for the baseline model (configuration G, see Figure 4) was as follows: molecules per release = 2000, total transporter molecules ($G_{1\text{-}2}$) = 2150, nonsynaptic source molecules = 38, with kinetic schemes as cited previously (see section 2.4), and all other parameters as reported in Table 1. By having all parameter values

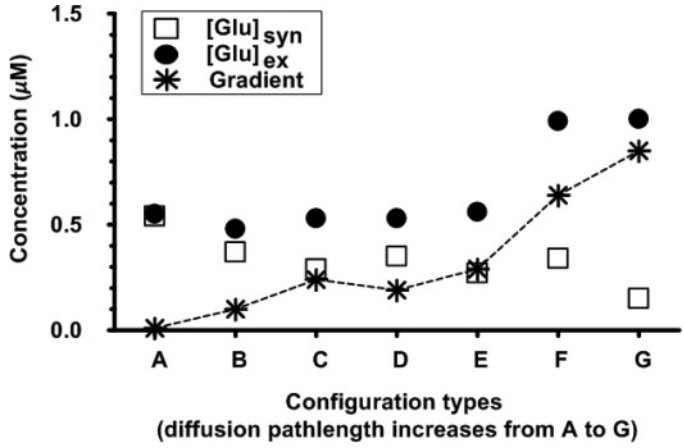

Figure 5: Comparison of $[Glu]_{syn}$ and $[Glu]_{ex}$ under control basal conditions for various glial configurations shown in Figure 4, using the same set of parameters, with configuration G as the baseline model. As expected, porous glia (configuration A) with zero diffusion path length supported no neurotransmitter gradient. The dotted line connects the gradient ($[Glu]_{ex}$-$[Glu]_{syn}$) achieved by each of these configurations. The diffusion path length increased from configuration A to G, and this path length was correlated to the neurotransmitter gradient between the ECS and the synaptic cleft.

constrained as in the baseline model, the comparative study determined the relative effectiveness of configurations A to G in maintaining a specified neurotransmitter gradient.

Figure 5 shows the variation in $[Glu]_{syn}$ and $[Glu]_{ex}$ across all the glial configurations A to G in Figure 4. The dashed line in Figure 5 connects the concentration gradients ($[Glu]_{ex}$-$[Glu]_{syn}$) achieved by each of these configurations. As expected, for the porous geometry in configuration A, $[Glu]_{syn}$ and $[Glu]_{ex}$ was the same at 0.52 μM, resulting in no concentration gradient. For the one-sheath glial geometries (configurations B and C), $[Glu]_{syn}$ dropped from 0.37 to 0.29 μM, while $[Glu]_{ex}$ increased from 0.48 to 0.53 μM. For all the configurations considered, geometries with two glial sheaths (configurations D–G) showed the largest gradient (see Figure 5), thus suggesting that higher gradients were based on the amount of synaptic isolation the glia provides. For instance, $[Glu]_{syn}$ dropped from 0.35 to 0.15 μM going from configuration D to G (see Figure 5).

Furthermore, to compare different modeling approaches (stochastic versus continuum), we investigated differences in transporter efficiency between volume-populated (Pendyam et al., 2009) and surface-populated cases based on configuration G in Figure 4. The details of the volume population methodology used in the continuum case can be found in Pendyam

et al. (2009). Due to the volume population of glial transporters, the continuum model (Pendyam et al., 2009) provided more space between the glial sheaths for molecular diffusion—140 nm, which was 100 nm of the glial volume (50 nm on either side of an impermeable center line) and 40 nm for the ECS gap. This compared to only 40 nm, the ECS gap in the stochastic model. Thus, the volume-populated continuum model resulted in an approximately 100% increase in $[Glu]_{syn}$ and $[Glu]_{mGluR}$ (0.35 μM and 0.38 μM, respectively), while $[Glu]_{ex}$ rose by only 10% to 1.1 μM compared to the stochastic model. Although the continuum model maintained a concentration gradient between the synaptic and extracellular space, it did not establish the required model constraints. The cause for this was a 50% decrease in transporter efficiency in the volume-populated model.

4 Discussion

Neurotransmitter homeostasis was modeled using a three-dimensional stochastic diffusion model of an example cortico-accumbens synapse to provide molecular-level insights. Previous stochastic models of synaptic environments have not typically considered a nonsynaptic release site for glutamate or modeled neurotransmitter gradients, both of which were included in the models considered in this study. The example case synapse was further generalized to investigate the effect of diffusion path length (defined as the distance that a molecule travels from the synaptic cleft to the ECS) on synaptic isolation using several feasible glial geometries. The insights provided by the models are described next.

4.1 Stochastic Molecular Model Quantifies the Role of Nonsynaptic Neurotransmitter Sources in Control and Cocaine Conditions.

4.1.1 Homeostasis. By combining physiological values from the literature and empirically derived changes due to chronic cocaine, the example case cortico-accumbens model reproduced experimentally observed glutamate concentrations for various cases (see Table 2 for model constraints). The model further provided molecular-level details not predicted by the continuum-based approach (Pendyam et al., 2009). Specifically, by labeling glutamate from synaptic and nonsynaptic sources, the model showed that the nonsynaptic source contribution to the homeostatic extracellular concentration varied from 100% (approximately 4000 molecules total) in the control basal case to 84% (approximately 5000 molecules total) and 24% (approximately 12000 molecules total) in the control natural reward and cocaine drug-seeking cases, respectively. This study established that only nonsynaptic sources maintained homeostatic concentration levels in the control basal condition for such synapses and acted as the source for the steady influx of molecules from the ECS to the perisynaptic environment. The model also shed light on experimental estimates of steady-state

concentrations measured in the synapse that may be due to the intermittent presence of a single glutamate molecule. Such a finely grained view of molecular activity in steady state is not feasible using continuum approaches.

4.1.2 Receptor Activity. The model also provided molecular insights related to the percentage of receptors (AMPA or NMDA) in the open state. In the control basal case, before a synaptic release, almost AMPA receptors were in the closed state. However, after a synaptic release, it was observed that although most of AMPA receptors were activated, they did not always result in AMPA receptors' reaching the open state. The choice of molecules released per synaptic firing, number of receptors in the synaptic cleft, D, glial geometry, and number of receptors in the perisynaptic vicinity plays an important role in shaping the characteristics of receptor activity. Although not the primary focus of this letter, the study showed that the receptor activity in the synaptic cleft during homeostasis was affected by synaptic and nonsynaptic sources of glutamate.

Also, the configuration in Figure 1 showed that with an average $[Glu]_{ex}$ of 4.79 μM, there was a constant influx of 5 molecules/ms from the ECS into the glial environment measured at the G_3 opening, between release events in the control basal case. As the molecules diffused toward the synaptic cleft from the opening in glial sheath G_3, the transporter-rich glial path reduced this flow of molecules from 5/ms to 2/ms near the mGluR2/3 region. The reduction in the number of molecules was caused by the uptake of diffusing molecules by the transporter-rich glial path.

As shown in Table 3, mGluR2/3 occupancy increased to 100% during cocaine drug-seeking conditions. The steady-state $[Glu]_{ex}$ in the cocaine drug-seeking case was approximately three times higher compared to the control basal case. Combined with the downregulation of glial transporters by 40%, it resulted in an increased influx of glutamate molecules from ECS, rendering mGluR2/3 ineffective. By comparing $[Glu]_{mGluR}$, mGluR occupancy, with release probabilities, an interesting observation was that steady-state mGluR occupancy was dependent on synaptic firing frequency and release and possibly slower Glu-mGluR2/3 binding kinetics. It should be noted that a higher mGluR2/3 occupancy in control natural rewards would result in suppression of synaptic release, whereas the high numbers in cocaine drug seeking are representative of a lack of presynaptic firing inhibition. In conclusion, the computational model structure enabled molecular-level quantification of the contribution of nonsynaptic glutamate sources to the regulation of homeostasis and receptor activity.

4.2 Glial Glutamate Transporters Had the Largest Effect on Glutamate Concentrations. The signs on the various perturbation numbers in Table 4 followed expected biological trends during steady-state conditions. By considering changes in glutamate concentrations from the nominal values at

Table 4: Normalized Perturbation Analysis to Rank the Parameters for the Example Case Cortico-Accumbens Synapse in Figure 1.

Parameters	Steady-State Glutamate Concentrations[a]	
	$[Glu]_{syn}$	$[Glu]_{ex}$
Transporters (molecules)	1.00	1.00
Diffusion ($\mu m^2/ms$)	−0.54	0.34
xc- (molecules)	−0.23	−0.86
Number of molecules per release (molecules)	0.01	−0.01
mGluR2/3 (molecules)	−0.04	0.03

[a]The signs indicate direction of change when the parameter varied from −10% to +10% around the model values listed in Table 1.

the three locations for the configuration in Figure 1, total transporters were found to be most important parameter in controlling $[Glu]_{syn}$ and $[Glu]_{ex}$. Counter to intuition, it was found that independently varying transporters by ±10% on glial sheath G_3 (see section 3) had a greater effect on $[Glu]_{syn}$ as compared to a similar change on G_1. Another observation was that around the nominal operating point, variation of ±10% in nonsynaptic source molecules was ranked second (after transporters) as far as its effect on $[Glu]_{ex}$ was concerned (see Table 4). Thus, the study helped highlight the role of glial sheaths and XAG in regulating molecular influx rates at a steady state that may be critical for perisynaptic receptor activity. These observations, although specific to the example case, should hold for other geometries that isolate the synapse and support neurotransmitter gradients.

4.3 Diffusion Path Length Correlates with Degree of Synaptic Isolation and Magnitude of Neurotransmitter Gradient. A generalized study of the example synapse was considered to characterize the role of glial geometry in supporting gradients and, subsequently, diffusion path length—in other words, which of the configurations in Figure 4 (with baseline model being configuration G, and $[Glu]_{ex} = 1\ \mu M$) yielded the largest gradient?

As expected, it was found that the porous glial geometry of configuration A could not support neurotransmitter concentration gradients, as shown in Figure 5. The one-sheath glial configuration (B and C in the figure) showed that a structured glial configuration ensured better utilization of transporters as compared to configuration A. This was reflected by the increased concentration gradient as shown in Figure 5. Configurations D and E represented the two-sheath versions of configurations B and C. As seen in Figure 5, by comparing configurations D and E, it was observed that while $[Glu]_{syn}$ decreased, there was a corresponding increase in $[Glu]_{ex}$. Thus, by increasing the interaction of the diffusing molecules with transporters, configurations D and E supported higher neurotransmitter gradient as compared to

their corresponding one-sheath models B and C. Interestingly, in spite of having just one glial sheath, configuration C maintained a higher gradient than D. This highlighted the importance of regulating molecular flow to the synapse, which helped maintain a gradient between the synapse and extracellular space. The dashed line in Figure 5 summarized the finding in this comparative study, that is, for the same set of parameters, diffusion path length was proportional to the gradient supported.

A comparative analysis of transporter efficiency revealed that volume-populating transporters (continuum approach) were found to be 50% less efficient compared to the surface-populated case (stochastic approach) for baseline configuration G. This was because the volume population of transporters in space compartments made them less concentrated and, hence, less efficient (i.e., the uptake rate decreased). The results suggested that by reducing the size of the space compartments, the continuum model would better approximate the surface-populated stochastic model, as others have noted (Stiles & Bartol, 2001; Franks et al., 2002).

4.4 Limitations. As cited, glial configurations and diffusion very close to synapses (approximately 1 μm) are not well understood, particularly for synapses that support gradients between the cleft and the ECS. Hence, the glial configurations considered should be viewed as being equivalent only in that they provide the same resistance to the flow of neurotransmitter observed in vivo. Second, the example case synapse considered only one neurotransmitter and stimulation of several of its receptors. Finally, the iterative process proposed could be used to determine alternate glial configurations with different XAG and xc- densities to satisfy all constraints simultaneously for changes to any of the assumptions made in this study. For instance, steady-state mGluR2/3 occupancy in the cortico-accumbens synapse was assumed to be 85%. If a different value is to be tested, the iterative methodology proposed could be used to determine appropriate parameter estimates for the configuration.

Future studies could also examine the effect of synaptic plasticity, including potentiation and depression of release probability, during trains of action potentials. This would be relevant to modeling addiction-related neuropathology since the ability to either potentiate or depotentiate synapses is attenuated at accumbens glutamatergic synapses after withdrawal from cocaine (Martin, Chen, Hopf, Bowers, & Bonci, 2006; Moussawi et al., 2009). The model could also incorporate other neurotransmitters, such as dopamine and GABA, that might additionally modulate the homeostatic mechanisms. Indeed, both dopamine and GABA transmission are altered followed chronic cocaine administration (Xi et al., 2003; Volkow et al., 2006), and modeling their influences on excitatory transmission should reveal a more complete portrait of cocaine-induced neuropathologies (Sun, Milovanovic, Zhao, & Wolf, 2008).

5 Conclusion

A biophysically realistic stochastic modeling framework was proposed to study neurotransmitter homeostasis around a class of synapses that supported neurotransmitter gradients. An example case of a cortico-accumbens synapse in control and cocaine conditions was considered to obtain molecular-level insights, including how nonsynaptic sources affected homeostasis. By incorporating cystine-glutamate exchanger as a nonsynaptic release site for glutamate, the model showed how cocaine-induced neuroadaptations influence glutamate transmission at accumbens synapses. This study provided another approach to validate the prediction of cocaine-induced downregulation of the glial glutamate transporter. The generalized models of the example case that were also considered shed light on the role of glial configurations in maintaining neurotransmitter gradients. While porous approximations of the neuropil could describe only the average behaviors of molecules, the configurations considered showed that glial geometries had characteristic diffusion path lengths that were correlated to the achievable gradients. Thus, such modeling approaches provide guidance about glial morphology around a class of synapses the support neurotransmitter gradients.

Acknowledgments

We thank Markus Dittrich, Pittsburgh Supercomputing Center, for providing assistance with the MCell software and for helpful comments on an earlier draft. We also thank the two anonymous reviewers for their comments, which helped improve the manuscript. This research was supported in part by USPHS grants DA015369, DA03906 (P. W. K.), and a subcontract from DA015369 and PSC grant IBN090001P to the University of Missouri (S.S.N.).

References

Alagarsamy, S., Sorensen, S. D., & Conn, P. J. (2001). Coordinate regulation of metabotropic glutamate receptors. *Cur. Op. Neurobiol., 11,* 357–362.

Attwell, D., & Gibb, A. (2005). Neuroenergetics and the kinetic design of excitatory synapses. *Nat. Rev. Neurosci., 6,* 841–849.

Baker, D. A., McFarland, K., Lake, R. W., Shen, H., Tang, X. C., Toda, S., et al. (2003). Neuroadaptations in cystine-glutamate exchange underlie cocaine relapse. *Nat. Neurosci., 6,* 743–749.

Barbour, B. (2001). An evaluation of synapse independence. *J. Neurosci., 21,* 7969–7984.

Bergles, D. E., & Jahr, C. E. (1997). Synaptic activation of glutamate transporters in hippocampal astrocytes. *Neuron, 19,* 1297–1308.

Billups, B., Graham, B. P., Wong, A. Y., & Forsythe, I. D. (2005). Unmasking group III metabotropic glutamate autoreceptor function at excitatory synapses in the rat CNS. *J. Physiol., 565,* 885–896.

Bruns, D., & Jahn R. (1995). Real-time measurement of transmitter release from single synaptic vesicles. *Nature, 377,* 62–65.

Cavelier, P., Hamann, M., Rossi, D., Mobbs, P., & Attwell, D. (2005). Tonic excitation and inhibition of neurons: Ambient transmitter sources and computational consequences. *Prog. Biophys. Mol. Biol., 87,* 3–16.

Chang, J. Y., Zhang, L., Janak, P. H., & Woodward, D. J. (1997). Neuronal responses in prefrontal cortex and nucleus accumbens during heroin self-administration in freely moving rats. *Brain Res., 754,* 12–20.

Clements, J. D. (1996). Transmitter time course in the synaptic cleft: Its role in central synaptic function. *Trends in Neuroscience, 19,* 163–171.

Clements, J. D., Robin, A., Lester, J., Tong, G., Jahr, C. E., & Westbrook G. L. (1992). The time course of glutamate in the synaptic cleft. *Science, 258,* 1498–1501.

Conrad, K. L., Tseng, K. Y., Uejima, J. L., Reimers, J. M., Hen, L. J., Shaham, Y., et al. (2008). Formation of accumbens GluR2-lacking AMPA receptors mediates incubation of cocaine seeking. *Nature*, 454(7200), 118–121.

Czech, J., Dittrich, M., & Stiles, J. R. (2009). Rapid creation, Monte Carlo simulation, and visualization of realistic 3D cell models. In I. V. Maly (Ed.), *Methods in molecular biology, systems biology* (pp. 237–287). Clifton, NJ: Humana Press.

Danbolt, N. C. (2001). Glutamate uptake. *Prog. Neurobiol., 65,* 1–105.

Diamond, J. S. (2005). Deriving the glutamate clearance time course from transporter currents in CA1 hippocampal astrocytes: Transmitter uptake gets faster during development. *J. Neurosci., 25,* 2906–2916.

Franks, K. M., Bartol, T. M., & Sejnowski, T. J. (2002). A Monte Carlo model reveals independent signaling at central glutamatergic synapses. *Biophys. J., 83,* 2333–2348.

Geiger, J. R. P., Roth. A., Taskin, B., & Jonas, P. (1999). Glutamate-mediated synaptic excitation of cortical interneurons. In P. Jonas & H. Monyer (Eds.), *Ionotropic glutamate receptors in the CNS: Handbook of experimental pharmacology* (pp. 363–398). Berlin: Springer-Verlag.

Haydon, P. (2001). Glia: Listening and talking to the synapse. *Nat. Neurosci., 2,* 2185–2191.

Herman, M. A., & Jahr, C. E. (2007). Extracellular glutamate concentration in hippocampal slice. *J. Neurosci., 27,* 9736–9741.

Holmes, W. R. (1995). Modeling the effect of glutamate diffusion and uptake on NMDA and non-NMDA receptor saturation. *Biophys. J., 69,* 1734–1747.

Hrabe, J., Harbetova, S., & Segeth, K. (2004). A model of effective diffusion and tortuosity in the extracellular space of the brain. *Biophys. J., 87,* 1606–1617.

Jonas, P., Major, G., & Sakmann, B. (1993). Quantal components of unitary EPSCs at the mossy fibre synapse on CA3 pyramidal cells of rat hippocampus. *J. Physiol., 472,* 615–663.

Kalivas, P. W. (2009). The glutamate homeostasis hypothesis of addiction. *Nat. Rev. Neurosci., 10,* 561–572.

Kalivas, P. W., Volkow, N., & Seamans, J. (2005). Unmanageable motivation in addiction: Pathology in prefrontal–accumbens glutamate transmission. *Neuron, 45,* 647–650.

Kau, K. S., Madayag, A., Mantsch, J. R., Grier, M. D., Abdulhameed, O., & Baker, D. A. (2008). Blunted cystine-glutamate antiporter function in the nucleus accumbens promotes cocaine-induced drug seeking. *Neuroscience, 155*, 530–537.

Kerr, R. A., Bartol, T. M., Kaminsky, B., Dittrich, M., Chang, J. C., Baden, S. B., et al. (2008). Fast Monte Carlo simulation methods for biological reaction—diffusion systems in solution and on surfaces. *S.I.A.M. J. Sci. Comp., 30(6),* 3126–3149.

Kleinle, J., Vogt, K., Luscher, H. R., Muller, R., Senn, W., Wyler, K., et al. (1996). Transmitter concentrations profiles in the synaptic cleft: An analytical model of release and diffusion. *Biophys. J., 71,* 2413–2426.

Knackstedt, L. A., Melendez, R. I., & Kalivas, P. W. (2010). Ceftriaxone restores glutamate homeostasis and prevents relapse to cocaine seeking. *Biol. Psychiatry, 67*, 81–84.

Koob, G. F., & Le Moal, M. (2001). Drug addiction, dysregulation of reward, and allostasis. *Neuropsychopharmacology, 24*, 97–129.

Kourrich, S., Rothwell, P. E., Klug, J. R., & Thomas, M. J. (2007). Cocaine experience controls bidirectional synaptic plasticity in the nucleus accumbens. *J. Neurosci., 27,* 7921–7928.

Lehre, K. P., & Danbolt, N. C. (1998). The number of glutamate transporter subtype molecules at glutamatergic synapses: Chemical and stereological quantification in young adult rat brain. *J. Neurosci., 18,* 8751–8757.

Lehre, K. P., & Rusakov, D. (2002). Asymmetry of glia near central synapse favors presynaptically directed glutamate escape. *Biophys. J., 83*, 125–134.

Le Meur, K., Galante, M., Anulo, M. C., & Audinat, E. (2007). Tonic activation of NMDA receptors by ambient glutamate of non-synaptic origin in the rat hippocampus. *J. Physiol., 580,* 373–383.

Lester, R. A., & Jahr, C. E. (1992). NMDA channel behavior depends on agonist affinity. *J. Neurosci., 12,* 635–643.

Martin, M., Chen, B. T., Hopf, F. W., Bowers, M. S., & Bonci, A. (2006). Cocaine self-administration selectively abolishes LTD in the core of the nucleus accumbens. *Nat. Neurosci., 9*, 868–869.

McFarland, K., Davidge, S. B., Lapish, C. C., & Kalivas, P. W. (2004). Limbic and motor circuitry underlying footshock–induced reinstatement of cocaine-seeking behavior. *J. Neurosci., 24,* 1551–1560.

McFarland, K., Lapish, C. C., & Kalivas, P. W. (2003). Prefrontal glutamate release into the core of the nucleus accumbens mediates cocaine-induced reinstatement of drug-seeking behavior. *J. Neurosci., 23,* 3531–3537.

Melendez, R. I., Vuthiganon J., & Kalivas, P. W. (2005). Regulation of extracellular glutamate in the prefrontal cortex: Focus on the cystine-glutamate exchanger and group I metabotropic glutamate receptors. *J. Pharmacol. Exp. Ther., 314,* 139–147.

Moran, M. M., McFarland, K., Melendez, R. I., Kalivas, P. W., & Seamans, J. K. (2005). Cystine/glutamate exchange regulates metabotropic glutamate receptor presynaptic inhibition of excitatory transmission and vulnerability to cocaine seeking. *J. Neurosci., 21,* 207–215.

Moussawi, K., Pacchioni, A., Moran, M., Olive, M. F., Gass, J. T., Lavin, A., et al. (2009). N-acetylcysteine reverses cocaine-induced metaplasticity. *Nat. Neurosci., 12*, 182–189.

Murthy, V. N., & Sejnowski, T. J. (1997). Heterogeneous release properties of visualized individual hippocampal synapses. *Neuron, 18*, 599–612.

Nicholson, C. (2001). Diffusion and related transport mechanism in brain tissue. *Reports on Progress in Physics, 64*, 815–884.

Nicholson, C., & Sykova, E. (1998). ECS structure revealed by diffusion analysis. *Trends in Neuroscience, 21*, 207–215.

Parsons, C. G., Danysz, W., & Zieglgansberger, W. (2005). Excitatory amino acid neurotransmission. *Handbook Exp. Pharmacol., 169*, 249–303.

Patneau, D. K., & Mayer, M. L. (1990). Structure-activity relationships for amino acid transmitter candidates acting at N-methyl-D-aspartate and quisqualate receptors. *J. Neurosci., 10*, 2385–2399.

Pendyam, S., Mohan, A., Kalivas, P. W., & Nair, S. S. (2009). Computational model of extracellular glutamate in the nucleus accumbens incorporates neuroadaptations by chronic cocaine. *Neuroscience, 158*, 1266–1276.

Robinson, T. E., & Kolb, B. (1999). Alterations in the morphology of dendrites and dendritic spines in the nucleus accumbens and prefrontal cortex following repeated treatment with amphetamine or cocaine. *Eur. J. Neurosci., 11*, 1598–604.

Rollenhagen, A., & Lubke, J. H. R. (2006). The morphology of excitatory central synapses: From structure to function. *Cell Tissue Res., 326*, 221–237.

Rusakov, D. A. (2001). The role of perisynaptic glial sheaths in glutamate spillover and extracellular Ca^{2+} depletion. *Biophys. J., 81*, 1947–1959.

Rusakov, D. A., & Kullmann, D. M. (1998). Extrasynaptic glutamate diffusion in the hippocampus: Ultrastructural constraints, uptake, and receptor activation. *J. Neurosci., 18*, 3158–3170.

Saftenku, E. E. (2005). Modeling of slow glutamate diffusion and AMPA receptor activation in the cerebellar glomerulus. *J. Theo. Bio., 234*, 363–382.

Savtchenko, L. P., & Rusakov, D. A. (2007). The optimal height of the synaptic cleft. *Proc. Natl. Acad. Sci. USA, 104*, 1823–1828.

Schoepp, D. D., & True, R. A. (1992). 1S, 3R-ACPD-sensitive (metabotropic) [^{3}H] glutamate receptor binding in membranes. *Neurosci. Lett., 145*, 100–104.

Stiles, J. R., & Bartol, T. M. (2001). Monte Carlo methods for stimulating realistic synaptic microphyiology using MCell. In E. De Schutter (Ed.), *Computational neuroscience: Realistic modeling for experimentalists* (pp. 87–127). Boca Raton, FL: CRC Press.

Stiles, J. R., Van Helden, D., Bartol, T. M. Jr., Salpeter, E. E., & Salpeter, M. M. (1996). Miniature endplate current rise times <100 μs from improved dual recordings can be modeled with passive acetylcholine diffusion from a synaptic vesicle. *Proc. Natl. Acad. Sci. USA, 93*, 5747–5752.

Sun, X., Milovanovic, M., Zhao, Y., & Wolf, M. E. (2008). Acute and chronic dopamine receptor stimulation modulates AMPA receptor trafficking in nucleus accumbens neurons cocultured with prefrontal cortex neurons. *J. Neurosci., 28*, 4216–4230.

Sun, W., & Rebec, G. V. (2006). Repeated cocaine self-administration alters processing of cocaine-related information in rat prefrontal cortex. *J. Neurosci., 26*, 8004–8008.

Sykova, E. (1997). The ECS in the CNS: Its regulation, volume and geometry in normal and pathological neural function. *Neuroscientist, 3,* 28–41.

Sykova, E. (2004). Extrasynaptic volume transmission and diffusion parameters of the ECS. *Neuroscience, 129,* 861–876.

Szumlinski, K. K., Abernathy, K. E., Oleson, E. B., Kullmann, M., Lominac, K. D., He, D. Y., et al. (2006). Homer isoforms differentially regulate cocaine-induced neuroplasticity. *Neuropsychopharmacology, 4,* 768–777.

Tao, L., & Nicholson, C. (2004). Maximal geometrical hindrance to diffusion in brain ECS surrounding uniformly spaced convex cells. *J. Theo. Bio., 229,* 59–68.

Tao, A., Tao, L., & Nicholson, C. (2005). Cell cavities increase tortuosity in brain extracellular space. *J. Theo. Bio., 234,* 525–536.

Thomas, M. J., Beurrier, C., Bonci, A., & Malenka, R. C. (2001). Long term depression in the nucleus accumbens: A neural correlate of behavioral sensitization to cocaine. *Nat. Neurosci., 4,* 1217–1223.

Thorne, R. G., & Nicholson, C. (2006). In vivo diffusion analysis with quantum dots and dextrans predicts the width of brain ECS. *Proc. Natl. Acad. Sci. USA, 103*, 5567–5572.

Timmerman, W., & Westerink, B. H. (1997). Brain microdialysis of GABA and glutamate: What does it signify? *Synapse, 27,* 242–261.

Trantham, H., Szumlinski, K., McFarland, K., Kalivas, P. W., & Lavin, A. (2002). Repeated cocaine administration alters the electrophysiological properties of prefrontal cortical neurons. *Neuroscience, 113,* 749–757.

Volkow, N. D., Wang, G. J., Telang, F., Fowler, J. S., Logan, J., Childress, A. R., et al. (2006). Cocaine cues and dopamine in dorsal striatum: Mechanism of craving in cocaine addiction. *J. Neurosci., 26*, 6583–6588.

Volynski, K. E., Rusakov, D. A., & Kullmann, D. M. (2006). Presynaptic fluctuations and release-independent depression. *Nat. Neurosci., 9,* 1091–1093.

Wadiche, J. I., Arriza, J. L., Amara, S. G., & Kavanaugh, M. P. (1995). Kinetics of a human glutamate transporter. *Neuron, 14,* 1019–1027.

Wolf, J. A., Moyer, J. T., Lazarewicz, M. T., Contreras, D., Benoit-Marand, M., O'Donnell, P., et al. (2005). NMDA/AMPA ratio impacts state transitions and entrainment to oscillations in a computational model of nucleus acumens medium spiny projection neuron. *J. Neurosci., 25,* 9080–9095.

Xi, Z. X., Baker, D. A., Shen, H., Carson, D. S., & Kalivas, P. W. (2002). Group II metabotropic glutamate receptors modulate extracellular glutamate in the nucleus accumbens. *J. Pharmacol. Exp. Ther., 300*, 162–171.

Xi, Z. X., Ramamoorthy, S., Shen, H., Lake, R., Samuvel, D. J., & Kalivas, P. W. (2003). GABA transmission in the nucleus accumbens is altered after withdrawal from repeated cocaine. *J. Neurosci., 23*, 3498–3505.

Zheng, K., Scimemi, A., & Rusakov, D. A. (2008). Receptor actions of synaptically released glutamate: The role of transporters on the scale from nanometers to microns. *Biophys. J., 95*, 4584–4596.

Received July 24, 2009; accepted August 21, 2010.